CCS Chemistry

RESEARCH ARTICLE

Received: May 21, 2023 | Accepted: July 24, 2023 | Published: Aug. 17, 2023

On-Surface Stereochemical Characterization of a Highly Curved Chiral Nanographene by Noncontact Atomic Force Microscopy and Scanning Tunneling Microscopy

Qigang Zhong[1†], Viktor Barát[2†], Dániel Csókás[3†], Kaifeng Niu[4,5], Marcin Górecki[6], Animesh Ghosh[2], Jonas Björk[5], Daniel Ebeling[1], Lifeng Chi[4,7*], André Schirmeisen[1*] & Mihaiela C. Stuparu[2*]

[1]Institute of Applied Physics, Center for Materials Research (LaMa), Justus-Liebig University Giessen, 35392 Giessen, [2]School of Chemistry, Chemical Engineering and Biotechnology, Nanyang Technological University, 637371 Singapore, [3]Institute of Organic Chemistry, Research Center for Natural Sciences, H-1117 Budapest, [4]Jiangsu Key Laboratory for Carbon-Based Functional Materials and Devices, Institute of Functional Nano and Soft Materials, Soochow University, 215123 Suzhou, [5]Department of Physics, Chemistry and Biology, IFM, Linköping University, 58183 Linköping, [6]Institute of Organic Chemistry, Polish Academy of Sciences, 01-224 Warsaw, [7]Macao Institute of Materials Science and Engineering (MIMSE), MUST-SUDA Joint Research Center for Advanced Functional Materials, Macau University of Science and Technology, Taipa 999078, Macao

**Corresponding authors: chilf@suda.edu.cn; andre.schirmeisen@ap.physik.uni-giessen.de; mstuparu@ntu.edu.sg;*
[†]Q. Zhong, V. Barát, and D. Csókás contributed equally to this work.

Cite this: *CCS Chem.* **2023**, 5, 2888–2896
DOI: 10.31635/ccschem.023.202303065

A highly distorted chiral nanographene structure composed of triple corannulene-fused [5]helicenes is prepared with the help of the Heck reaction and oxidative photocyclization with an overall isolated yield of 28%. The complex three-dimensional (3D) structure of the bowl-helix hybrid nanostructure is studied by a combination of noncontact atomic force microscopy (AFM) and scanning tunneling microscopy (STM) on the Cu(111) surface, density functional theory calculations, AFM/STM simulations, and high-performance liquid chromatography-electronic circular dichroism analysis. This examination reveals a molecular structure in which the three bowl-shaped corannulene bladesd position themselves in a C_3-symmetric fashion around a highly twisted triphenylene core. The molecule appears to be shaped like a propeller in which the concave side of the bowls face away from the connected [5]helicene motif. The chirality of the nanostructure is confirmed by the direct visualization of both *MMM* and *PPP* enantiomers at the single-molecule level by scanning probe microscopies. These results underline that submolecular resolution imaging by AFM/STM is a powerful real-space tool for the stereochemical characterization of 3D curved chiral nanographene structures.

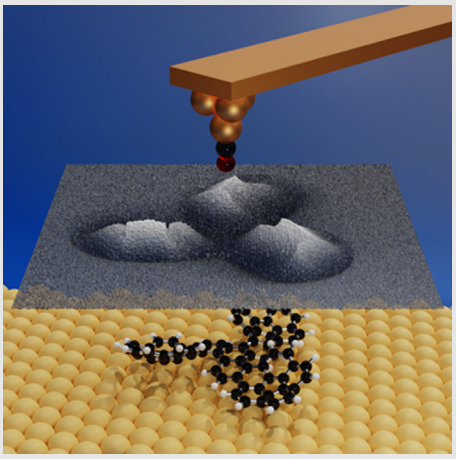

Keywords: **chirality at surfaces, noncontact atomic force microscopy, scanning tunnelling microscopy, submolecular resolution imaging, single-bond resolution, curved nanographenes, multiple helicenes, chiral nanostructures, bowl-helix hybrids, scanning probe microscopy**

Introduction

The research field of nanographenes has been growing rapidly[1–3] and in addition to typical planar molecules, a large variety of curved nanostructures[4–6] based on bowl,[7–12] saddle,[13–15] helix,[16–18] and belt[19] motifs have been prepared. Nonetheless, when the molecular dimensions and structural complexity increases, characterization of the molecular structure becomes a formidable challenge.[20,21] Although X-ray crystallography lends itself perfectly to the elucidation of the complex stereochemical structure in the solid phase, it may not always be applicable, as the crystallization of large molecules remains far from trivial. In such cases, alternative characterization techniques that do not rely upon intrinsic molecular properties would prove useful. Submolecular resolution imaging by scanning tunneling microscopy (STM) and atomic force microscopy (AFM) has the potential to become a powerful analytical tool in interpreting the intricate three-dimensional (3D) molecular structure in real space.[22] Using the conventional STM technique, for example, it is possible to differentiate between enantiomers of simple helicenes.[23] To determine the precise location of the atoms within arbitrary molecular nanostructures, the AFM bond imaging technique is required.[24–27] Therewith, for example, the absolute configuration of chiral aliphatic compounds can be identified by visual inspection, which allows studying chiral molecular recognition processes at the single-molecule level.[28,29] Furthermore, via the AFM method, it becomes possible to study adsorption conformations of 3D molecular structures. It allows, for example, to precisely measure twisting angles of individual carbon rings within a compound.[30–33] Submolecular resolution imaging, therefore, holds immense promise in studying molecular structure on surfaces. Its application to decipher the stereochemical structure at the single-molecule level in the arena of chiral nanographenes[34] is, however, severely restricted.[35–38] To this end, we show that a combination of submolecular resolution imaging, density functional theory (DFT) calculations, and AFM/STM simulations allow for the characterization of a novel corannulene-based chiral nanographene that could not be studied with the help of X-ray crystallography.

Our results indicate that the nanographene adopts a C_3-symmetric propeller-shaped geometry with three tilted corannulene blades fused to a homochiral triple [5]helicene motif. Moreover, the corannulene-[5]helicene hybrid motif adopts a predominant 3D geometry where the concave side of corannulene turns away from [5]helicene. This geometry corresponds to the most thermodynamically favorable diastereomer out of the 12 possible. The chirality of this configuration is confirmed by the identification of both *MMM* and *PPP* enantiomers. DFT calculations suggest that the curvature of corannulene enhances the distortion of [5]helicene, leading to a highly distorted molecular structure. In contrast, the molecular adsorption structure on the Cu(111) surface is substantially flattened due to strong molecule-surface interactions.

Experimental Methods

On-surface analysis

A clean Cu(111) surface was prepared in an ultra-high vacuum environment by cleaning the Cu(111) crystal (MaTecK, Germany) with repeated Ar^+ sputtering (6×10^{-6} mbar, 1.5 keV) and annealing (~800 K) cycles. The corannulene-based nanographene molecules were sublimated at 660 K by means of a commercial evaporator (Kentax, Germany) and deposited onto the clean Cu(111) surface held at about 6 K. The sample was then annealed at room temperature for 5 min to desorb the small impurities. Finally, the sample was loaded into the STM scanner held at 5.2 K. A few CO molecules were co-adsorbed on the surface for tip modification.

All the STM and AFM images were recorded at 5.2 K under ultra-high vacuum conditions (base pressure better than 1.0×10^{-10} mbar) using a combined STM/AFM system (Scienta Omicron, Germany). A tungsten tip was attached to a qPlus type force sensor to allow for simultaneous detection of tunneling current and atomic forces. The force sensor was controlled by a phase-locked loop electronics (MFLI, Zürich Instruments, Switzerland) in frequency modulation mode with key parameters: resonance frequency $f \approx 27.0$ kHz, quality factor $Q > 10{,}000$, oscillation amplitude $A = 52$ pm. Bias voltage was applied to the sample while the tip was grounded. The tip was conditioned on the Cu(111) surface by indentation (a few nanometers) and voltage pulses (–10 to 10 V); therefore, the tip was presumably to be covered by Cu atoms. To acquire atomic resolution in AFM imaging, the tip apex was modified with a single CO molecule by vertical manipulation of surface-adsorbed CO molecules with short voltage pulses (3.0 V, 500 ms). Successful tip modification manifested in the enhancement of STM image contrast and was further confirmed by frequency shift versus tip-sample distance spectroscopy on Cu(111).

Results and Discussion

The nanographene synthesis involves two simple synthetic steps (Scheme 1). Initially, iodocorannulene[39,40] was subjected to a palladium-catalyzed Heck reaction with 1,3,5-trivinylbenzene to give the precursor **1** in an isolated yield of 63%. A subsequent oxidative photocyclization led to the formation of nanographene **2** in an isolated yield of 45%. In **2**, the three corannulene units wre attached to a triphenylene core, and the overall structure

DOI: 10.31635/ccschem.023.202303065
Citation: *CCS Chem.* **2023**, 5, 2888–2896
Link to VoR: https://doi.org/10.31635/ccschem.023.202303065

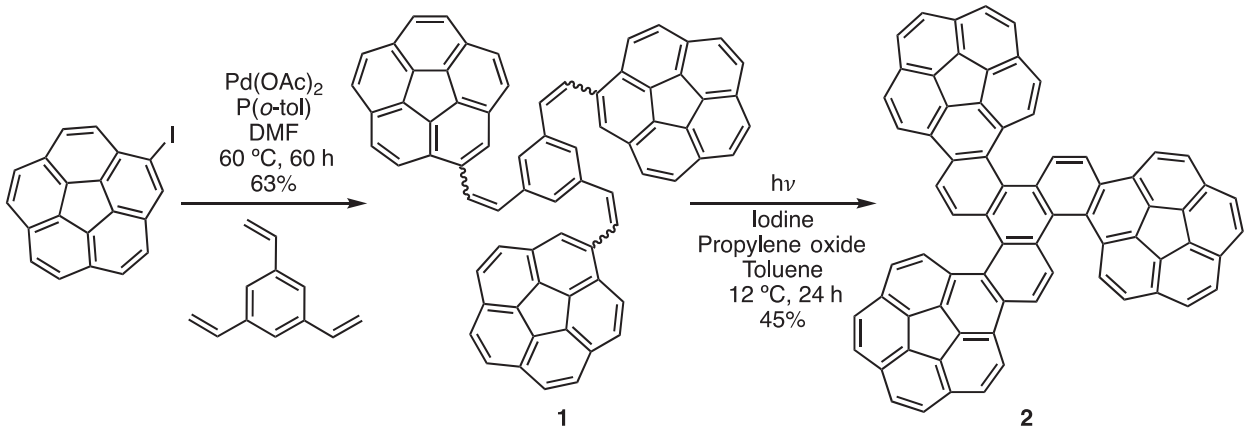

Scheme 1 | *Synthesis of curved π-system* ***2****.*

contained triple [5]helicenes.[41] In NMR spectroscopy (see Supporting Information Figures S1–S6), as expected, aromatic resonances shifted downfield upon formation of the triphenylene core. In UV–vis spectroscopy, **1** exhibits two broad absorption bands at 300 and 375 nm. In the case of **2**, a shoulder appears at 400 nm, presumably due to extension of π-conjugation upon photocyclization.

The molecular structure of **2** can be viewed as a triple corannulene-[5]helicene hybrid where the three [5]helicenes share a triphenylene core and are respectively fused with a corannulene bowl at the other termini by sharing two hexagons. The two-dimensional (2D) representation of **2** possesses threefold rotational symmetry; therefore, a corannulene-[5]helicene motif can represent the elemental 3D configurational features of **2**. This motif includes two nonplanar elements, that is, the bowl-shape of corannulene and the helicity of [5]helicene, where the inversion of either one will lead to diastereomerization as illustrated in Figure 1a–c.[42,43] Accordingly, there were two C_3-symmetric propeller-shaped diastereomers **2a** and **2b** and their enantiomers **2a*** and **2b*** (Figure 1b). The enantiomerization between **2a** (**2b**) and **2a*** (**2b***) required the inversions of all corannulenes and helicenes, while incomplete inversions could provide other 10 diastereomers with reduced symmetry and the corresponding enantiomers (see Supporting Information Figures S7–S14 and Table S1). **2** could not be coerced into yielding X-ray quality single crystals, which could be related to the complexity of the 3D configurations and active molecular dynamics. Therefore, to examine its stereochemical structure, we resorted to the power of submolecular resolution imaging of scanning probe microscopy.

For this, we deposited **2** onto atomically flat terraces of a Cu(111) surface via thermal evaporation and visually inspected the molecules with STM and AFM at 5.2 K under ultra-high vacuum conditions. We obtained a very low coverage of **2** on the Cu(111) surface among which nine molecules in total were imaged. This low coverage could be related to the instability of **2** at the high sublimation temperature required due to its large size ($C_{72}H_{30}$).

Figure 2a shows a typical STM image of an individual molecule **2** acquired with a metal (Cu) tip. The molecule appears to be a three-bladed propeller where the blades are brighter (higher) than the center. The diameter of the molecule was measured to be about 2.1 nm, which is in good agreement with the theoretical size of **2**.

We further achieved atomic resolution of the molecule by constant-current STM and AFM imaging with a CO-functionalized tip (Figure 2b,c). The topmost atoms are clearly depicted (marked with red arrows in Figure 2b), and the corannulene bowls are partially resolved (Figure 2c), whereas the lowest parts remain invisible. The constant-height AFM image in Figure 2g reveals that there are six atoms in the highest plane parallel to the substrate surface, that is, two atoms at each corannulene blade with the inner one appearing slightly brighter (higher) than the outer one. The second highest atoms emerged next to the highest six atoms during AFM scanning at closer tip-sample distance (see light blue arrows in Figure 2h). The remaining atoms at lower planes are difficult to resolve without causing damage to the tip or manipulating the molecule.

The observed image features are typical for hydrogen atoms that are pointing rather upwards; that is, the features are in good agreement with images from the literature where the C–H bond is either strongly rotated out of the surface plane or even, almost perpendicular to the surface.[28,44–46] This suggests that the concave side of the corannulene bowls is facing away from the surface.[47] Otherwise, parts of the carbon rings of the bowls should appear in the AFM images as it is the case for rather planar molecular structures. In our on-surface experiments, only the bowl-up adsorption structures were observed, which we ascribed to the strong interactions between the convex side of corannulene and the Cu

DOI: 10.31635/ccschem.023.202303065
Citation: *CCS Chem.* **2023**, 5, 2888–2896
Link to VoR: https://doi.org/10.31635/ccschem.023.202303065

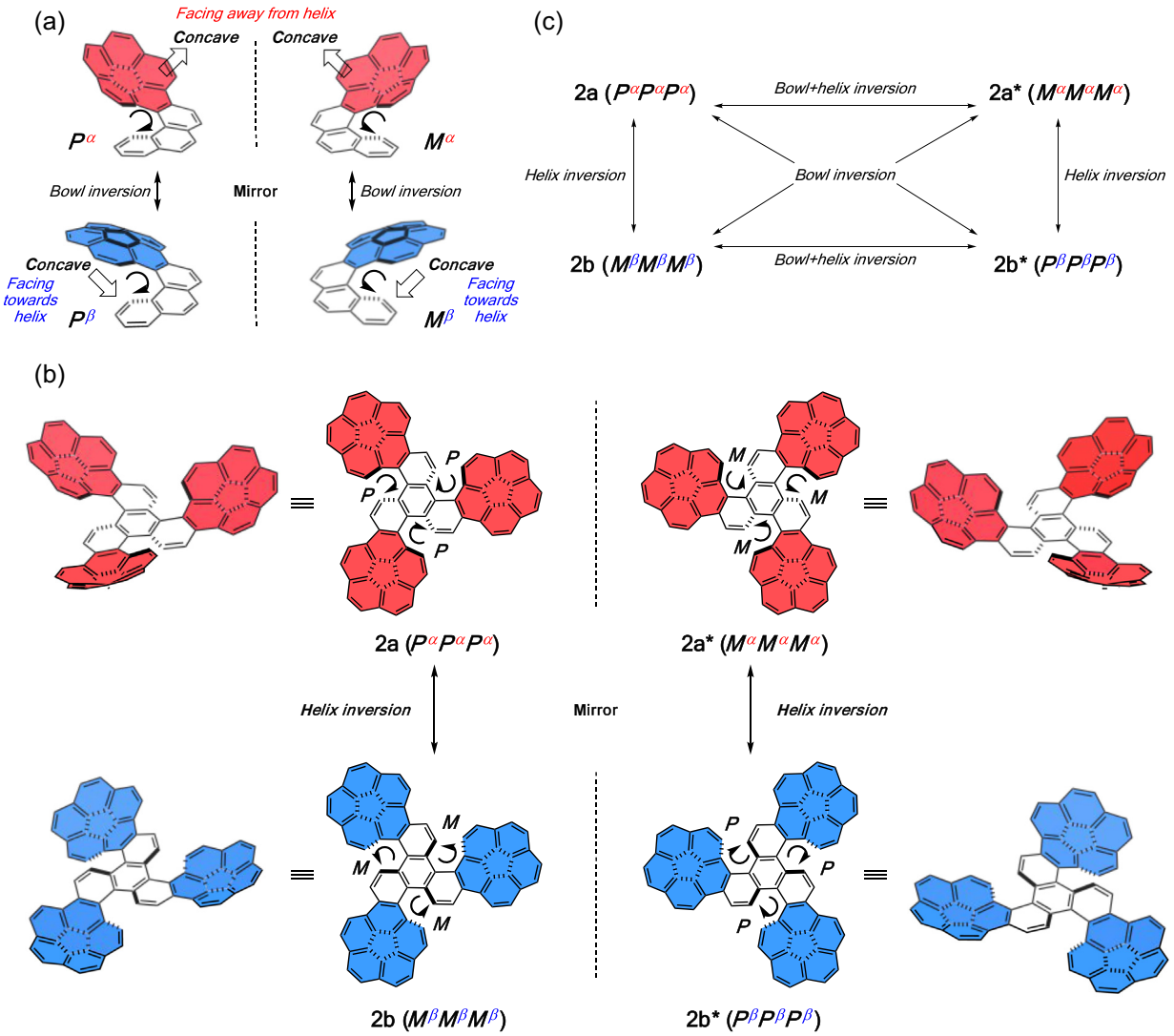

Figure 1 | *Steric configurations of nanographene **2**. (a) Two diastereomers of the corannulene-fused [5]helicene motif with the concave side of corannulene facing away from and towards the helix, respectively. (b, c) Two C_3-symmetric propeller-shaped conformers **2a** and **2b** out of 12 possible diastereomers of the corannulene–helicene hybrid molecule **2**. The helicity of the [5]helicene moieties (P or M) is annotated around the structural formulae. All the corannulene bowls have their concave side facing up. Configurations **2a*** and **2b*** are the respective enantiomers (mirror images) of **2a** and **2b**. The interconversion of diastereomers **2a** (**2a***) and **2b** (**2b***) can be realized by helicene inversions. It is of note that due to the mechanism of the interconversion, the helix inversion entails bowl inversion (i.e., P → M takes place along with α → β interconversion).*

surface.[47] In case the molecules of **2a** (**2a***) land on the Cu(111) surface in bowl-down configurations, they could presumably relax into more energetically stable bowl-up configurations at room temperature. The bowl-up adsorption structures are further stabilized under the cryogenic imaging conditions where the dynamic bowl inversions are forbidden.

Although the above measurements conform to the features of the energetically most stable conformation **2a** (*P*α*P*α*P*α) in the gas phase, the other C_3-symmetric diastereomer **2b*** of the same chirality (*PPP*) could not yet be excluded. To better understand this nonplanar molecular conformation, we performed vdW-DFT calculations[48] on the adsorption structures of **2a** (*P*α*P*α*P*α) and **2b*** (*P*β*P*β*P*β) on Cu(111). Conformer **2a** was found to be more stable than **2b*** by 0.90 and 0.56 eV in the gas phase and on the Cu(111) surface, respectively, (Supporting Information Figure S15), corresponding to the most thermodynamically stable diastereomer in solution (see Supporting Information Figure S12). Simulated STM (Figure 2d and Supporting Information Figure S16) and AFM (Figure 2j,k) images of **2a** based on the DFT calculations (Figure 2e,f) were highly consistent with the experimental results. In particular, the AFM

DOI: 10.31635/ccschem.023.202303065
Citation: *CCS Chem.* **2023**, 5, 2888–2896
Link to VoR: https://doi.org/10.31635/ccschem.023.202303065

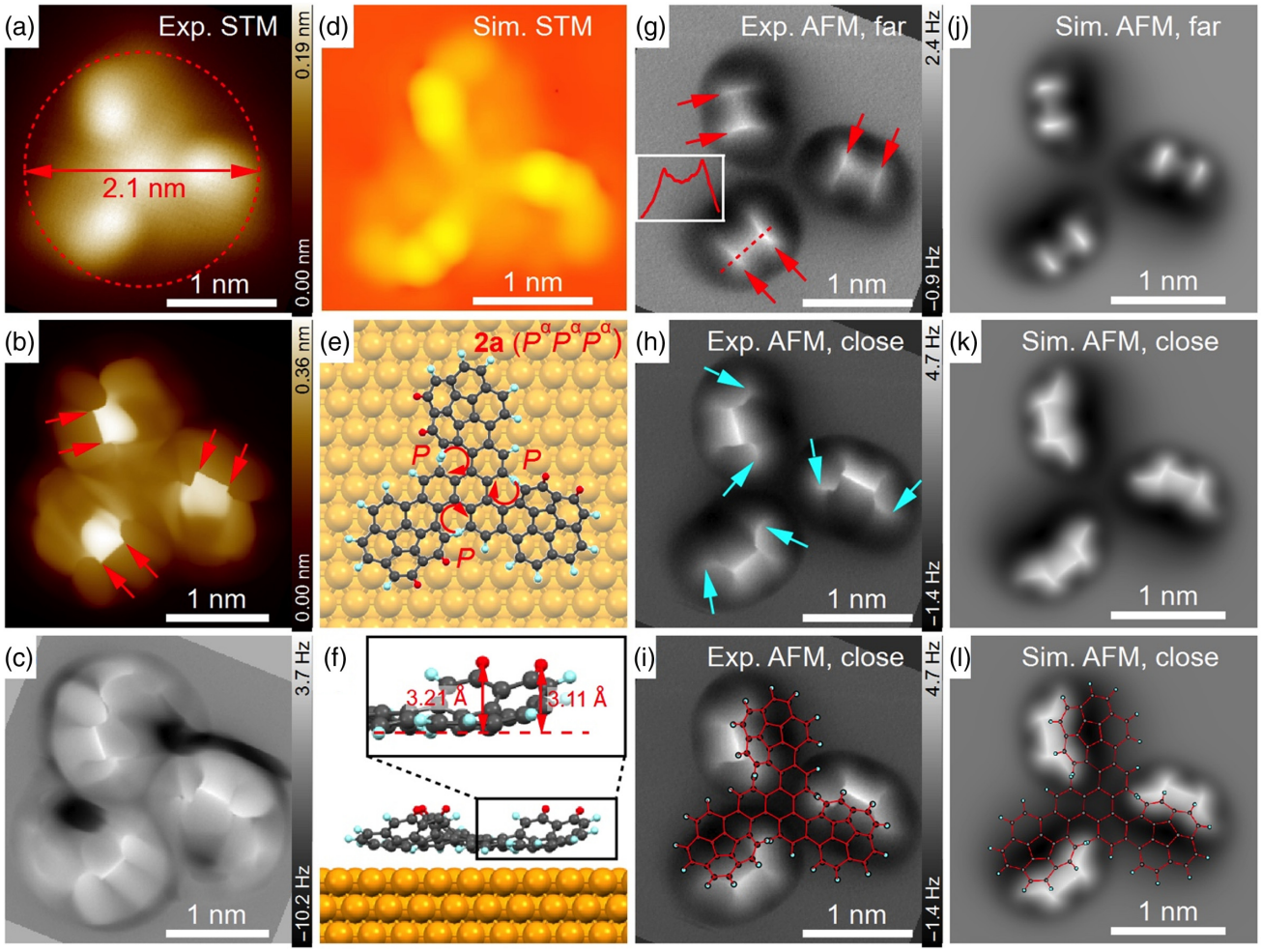

Figure 2 | *High resolution imaging of **2a** on Cu(111). (a) STM image of this molecule with a metal tip. (b, c) Constant-current bond-resolved STM and AFM images of an individual molecule **2a** using a CO-functionalized tip. (d) Simulated STM image of **2a** at an energy of 0.5 eV above the Fermi level. (e, f) Top and side views of the adsorption structure of **2a** on Cu(111). Color codes: C (grey), H (light blue or red), and Cu (orange). The hydrogen atoms shown in red are the highest atoms above the surface. (g, h) Experimental constant-height AFM images of the molecule **2a** at far and close tip-sample distances. The inset in (g) shows the line profile along the red dashed line from left to right. (i) The same image as (h) is superimposed with the structural model of **2a**. (j, k) Simulated constant-height AFM images of **2a** at far and close tip-sample distances. (l) The same image as (k) is superimposed with the structural model of **2a**. Imaging parameters: (a) 100 mV, 5 pA; (b, c) 10 mV, 30 pA; tip-sample distance offset Δz = +150 pm (g) and +100 pm (h), relative to 100 mV, 5 pA.*

simulations reproduce all the fingerprints of the highest and second highest atoms (hydrogen) within the molecule. The subtle height difference of 0.1 Å (Figure 2f) between the highest atoms was reproduced by both experimental and simulated AFM images (Figure 2g,j). Note that the sharp bond-like lines between the atoms in the STM and AFM images are artifacts due to the strong tilting of CO tips at close tip-sample distance.[49]

The optimized molecular models of surface-adsorbed **2a** were fitted to the AFM images in Figure 2i,l to locate the hydrogen atoms that contribute to the contrast. In contrast, the adsorption structure of **2b*** presented obvious discrepancies in comparison with the experiment. Specifically, for **2b*** the triphenylene unit was more strongly deformed in comparison with that of **2a** (see Supporting Information Figure S15), presumably due to increased steric hindrance by the periphery of the corannulene bowls bent towards it. Consequently, the topmost hydrogens of the triphenylene unit were almost as high as the red hydrogens of the corannulenes and, therefore, should appear with similar contrast in the AFM images (as shown by the AFM simulation in Supporting Information Figure S17), which, however, was not the case. Moreover, the two topmost hydrogen atoms at one

DOI: 10.31635/ccschem.023.202303065
Citation: *CCS Chem.* **2023**, 5, 2888–2896
Link to VoR: https://doi.org/10.31635/ccschem.023.202303065

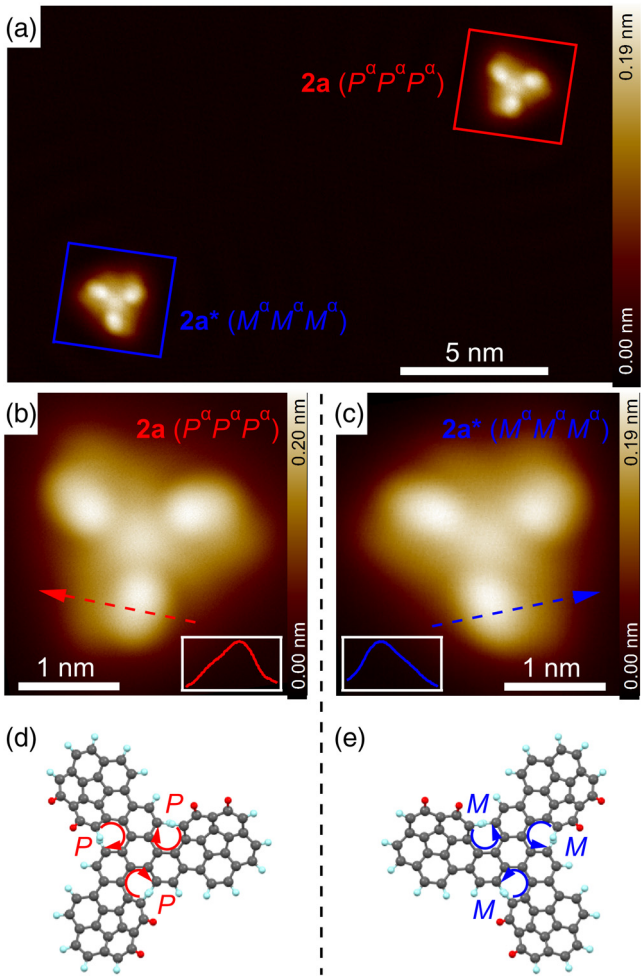

Figure 3 | *Visually distinguishing the enantiomers **2a** and **2a*** on Cu(111). (a) STM image of a **2a** and a **2a*** molecule. (b, c) Zoom-in STM images of the two molecules. The red/blue dashed arrows mark the tilting directions of the corannulene blades and the corresponding line profiles are shown as insets. (d, e) Molecular structures of the two enantiomers. The atoms are color-coded: C (grey), H (light blue or red). The hydrogen atoms shown in red are the highest atoms above the surface. Imaging parameters: (a–c) 100 mV, 5 pA.*

corannulene blade of **2b*** had an inverse relationship in adsorption height and the related C–H bonds point to different directions.

As illustrated in Figure 1b, the conformer **2a** itself possessed an inherent chirality arising from the introduction of curvature in the molecular structure of which the 2D representation bore no perpendicular symmetry planes.[50] This chirality was confirmed by capturing both enantiomers **2a** (*P*α*P*α*P*α) and **2a*** (*M*α*M*α*M*α) on the Cu(111) surface with STM. Figure 3a presents both enantiomers in the same frame. We can clearly identify the tilting (high and low parts) of the corannulene blades from the closeup STM images (Figure 3b,c), and assign the corresponding chiral molecular models to them (Figure 3d,e). More specifically, the key fingerprint to distinguish **2a** from **2a*** is the opposite tilting directions of their corannulene blades, as depicted by the red/blue dashed arrows and corresponding line profiles in Figure 3b,c.

More molecules have been visually scrutinized, which exhibit consistent topography (Supporting Information Figure S18). In total, five **2a*** (*M*α*M*α*M*α) and four **2a** (*P*α*P*α*P*α) molecules were imaged, suggesting that the synthesized compound is a racemic mixture. The dynamic enantiomerization of **2a** via the inversion of corannulene bowls and [5]helicenes was inhibited due to the stabilization by molecule-surface interactions and the insufficient activation energy under the imaging conditions (5.2 K). However, the interconversion between the enantiomers and between different diastereomers should be possible in solution at room temperature according to the calculated activation barriers (see Supporting Information Figure S14, 12.5 kcal/mol for bowl inversion and 22.9 kcal/mol for [5]helicene inversion).

DFT calculations enabled the quantitative analysis of the distortion of **2a** (Figure 4a,b). For **2a** in solution phase, the [5]helicenes exhibited a larger interplanar angle between the two terminal rings than that in pristine [5]helicene (65.2° vs 46.0°) arising from the fusion of bowl-shaped corannulene. Moreover, the triphenylene core is also twisted by steric congestion, with an average

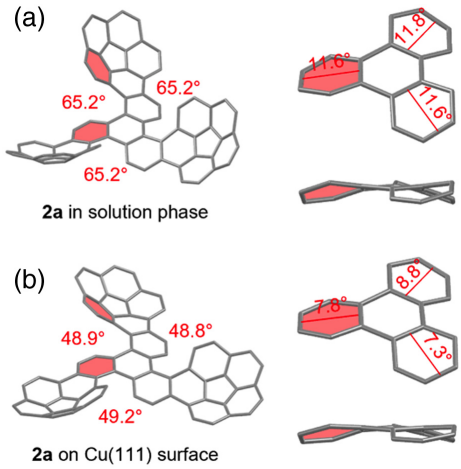

Figure 4 | *3D representations of **2a**. (a) Molecular structure of **2a** optimized at the ωB97X-D/def2SVP level of theory. (b) Optimized structure of **2a** adsorbed on Cu(111) via vdW-DFT calculation. Hydrogen atoms are omitted for clarity. The interplanar angles between the terminal rings (e.g., the two red-filled hexagons) of [5]helicenes are marked in red. The distorted triphenylene core of **2a** with torsion angles and the corresponding side view are displayed on the right of the panels.*

DOI: 10.31635/ccschem.023.202303065
Citation: *CCS Chem.* **2023**, 5, 2888–2896
Link to VoR: https://doi.org/10.31635/ccschem.023.202303065

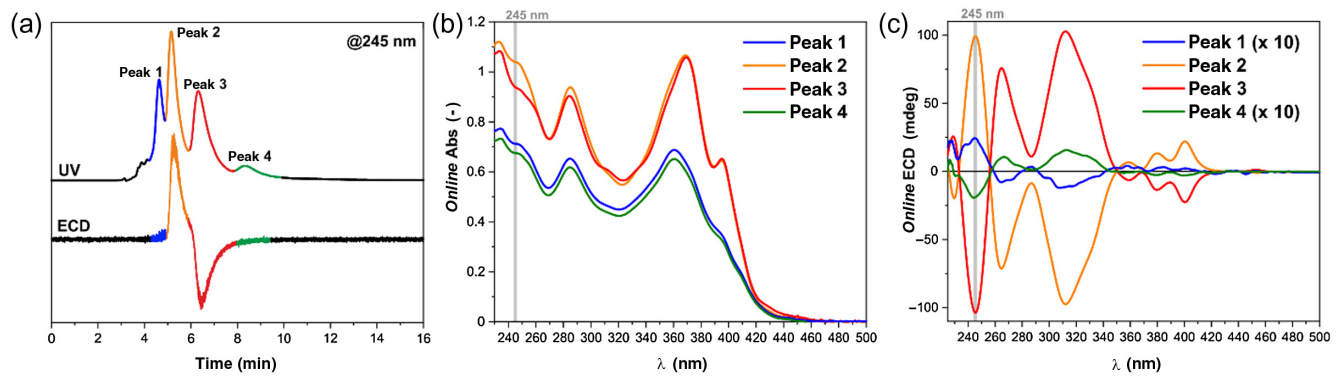

Figure 5 | *(a) UV (top) and ECD (bottom) chromatograms of **2** on a ReproSil Chiral-MIC column (n-Hex : DCM = 20:80, flow = 1 mL min^{-1}, temperature = 20 °C) detected at 245 nm; (b) online UV, and (c) online ECD spectra of eluted isomers of **2**. Note: UV/ECD spectra are normalized, and ECD recorded from peaks 1 and 4 are multiplied by 10 to confront them with data from peaks 2 and 3.*

torsion angle of 11.7° for the three outer rings. The curvature of this molecule is significantly attenuated upon its adsorption on Cu(111); that is, the interplanar angle and torsion angle were respectively reduced by about 25% and 32%, which we ascribed to the strong molecule-surface interactions, including van der Waals and chemical forces.[47]

Finally, to investigate the conformational landscape of **2** in the solution, we decided to carry out a high-performance liquid chromatography (HPLC)-electronic circular dichroism (ECD) analysis to detect and assign the structure of the most stable diastereomers in equilibrium. This approach to the stereochemical analysis of chiral compounds supported by quantum chemical calculations has been demonstrated to be highly effective and dependable for investigating the 3D structure of diverse chiral organic molecules.[51–53] Under our conditions of HPLC separation, four peaks were identified at 4.7, 5.3, 6.4, and 8.4 min, respectively (Figure 5a).

In ECD detection carried out at 245 nm, only the most intense peaks 2 and 3 give clear, opposite ECD signals. Nevertheless, we could record full ECD spectra for all peaks. The experimental *online* UV/ECD spectra from peaks were recorded in the course of HPLC separation, thanks to a manual stop-flow mode (Figure 5b,c). *Online* ECD spectra recorded from peaks 1 and 4 and peaks 2 and 3 show the mirror image relationship, which is characteristic for enantiomers. Furthermore, peaks 1 and 2, and peaks 3 and 4 exhibit the same sequence of Cotton effects, which indicate that they have the same configuration. However, the intensity of *online* ECD spectra substantially differ: peaks 1 and 4 are about 5–10 times lower in intensity to peaks 2 and 3. The ECD spectra recorded from peaks 1 and 4 are characterized by g_{abs} factors in the range from 1×10^{-4} to 4×10^{-5}, while peaks 2 and 3 are characterized by substantially higher values in the range of 3–5 × 10^{-3}. This clearly points out that two different pairs of species are present in the solution. Considering the issues related to the stability of the isomers of **2**, we also carried out the variable temperature (VT)-HPLC analysis using UV/ECD detection. In the range from 20 to 30 °C (see Supporting Information Figure S19), we did not observe any substantial changes, which indicates no detectable fluctuations of the conformational pool in the solution equilibrium within the investigated temperature range. However, further experiments by VT-NMR at higher temperatures (40 and 60 °C) in $CDCl_3$ confirmed that the dynamic interconversion begins at a higher temperature, notably broadening the peak of the minor diastereomer (see Supporting Information Figures S20 and S21).

The ECD spectra are not suitable for the differentiation of **2a** from **2b*** since ECD spectra are not sensitive enough to the bowl-face orientation of **2**. Nevertheless, the results indicate *MMM*-helicity for peaks 1 and 2 and *PPP*-helicity for peaks 3 and 4.

Conclusion

In conclusion, a combination of Heck reaction and photochemical cyclization involving appropriate corannulene halide and aryl vinylene precursors leads to the formation of a highly distorted propeller-shaped novel nanographene in an overall isolated yield of 28%. While single crystals could not be grown for X-ray crystallographic investigations, a combination of submolecular resolution imaging, DFT calculations, AFM/STM simulations, and HPLC-ECD analysis allow for the successful stereochemical characterization of this chiral 3D nanographene structure. Out of the possible 12 diastereomers our surface examination can identify one specific diastereomer. Both *MMM* and *PPP* enantiomers of this diastereoisomer could be visualized at the single-molecule level.

DOI: 10.31635/ccschem.023.202303065
Citation: *CCS Chem.* **2023**, 5, 2888–2896
Link to VoR: https://doi.org/10.31635/ccschem.023.202303065

Supporting Information

Supporting Information is available and includes experimental details and computational data.

Conflict of Interest

There is no conflict of interest to report.

Funding Information

Financial support from the Ministry of Education Singapore under the AcRF Tier 1 (MOE T1 RG11/21) and AcRF Tier 2 (MOE-T2EP10221-0002) is acknowledged. The Deutsche Forschungsgemeinschaft via grants (nos. SCHI 619/13 and EB535/1-1), the GRK (Research Training Group) 2204 "Substitute Materials for Sustainable Energy Technologies," the LOEWE Program of Excellence of the Federal State of Hesse (LOEWE Focus Group PriOSS "Principles of On-Surface Synthesis"), the National Natural Science Foundation of China (grant nos. 21790053, 51821002, and 22072103), the National Major State Basic Research Development Program of China (grant nos. 2017YFA0205000 and 2017YFA0205002), the Collaborative Innovation Center of Suzhou Nano Science & Technology, and the 111 Project are also acknowledged for their financial support. Computational resources were allocated at the National Supercomputer Centre, Sweden, by SNIC, and at the Wroclaw Centre for Networking and Supercomputing, Poland.

References

1. Pozo, I.; Guitián, E.; Pérez, D.; Peña, D. Synthesis of Nanographenes, Starphenes, and Sterically Congested Polyarenes by Aryne Cyclotrimerization. *Acc. Chem. Res.* **2019**, *52*, 2472–2481.
2. Narita, A.; Wang, X.; Feng, X.; Müllen, K. New Advances in Nanographene Chemistry. *Chem. Soc. Rev.* **2015**, *44*, 6616–6643.
3. Jolly, A.; Miao, D.; Daigle, M.; Morin, J.-F. Emerging Bottom-Up Strategies for the Synthesis of Graphene Nanoribbons and Related Structures. *Angew. Chem. Int. Ed.* **2020**, *59*, 4624–4633.
4. Majewski, M. A.; Stępień, M. Bowls, Hoops, and Saddles: Synthetic Approaches to Curved Aromatic Molecules. *Angew. Chem. Int. Ed.* **2019**, *58*, 86–116.
5. Segawa, Y., Ito, H.; Itami, K. Structurally Uniform and Atomically Precise Carbon Nanostructures. *Nat. Rev. Mater.* **2016**, *1*, 1–14.
6. Zhang, Y.; Pun, S. H.; Miao, Q. The Scholl Reaction as a Powerful Tool for Synthesis of Curved Polycyclic Aromatics. *Chem. Rev.* **2022**, *122*, 14554–14593.
7. Tsefrikas, V. M.; Scott, L. T. Geodesic Polyarenes by Flash Vacuum Pyrolysis. *Chem. Rev.* **2006**, *106*, 4868–4884.
8. Scott, L. T. Fragments of Fullerenes: Novel Syntheses, Structures and Reactions. *Pure Appl. Chem.* **2009**, *68*, 291–300.
9. Wu, Y. T.; Siegel, J. S. Aromatic Molecular-Bowl Hydrocarbons: Synthetic Derivatives, Their Structures, and Physical Properties. *Chem. Rev.* **2006**, *106*, 4843–4867.
10. Sygula, A. Chemistry on a Half-Shell: Synthesis and Derivatization of Buckybowls. *Eur. J. Org. Chem.* **2011**, *2011*, 1611–1625.
11. Stępień, M. Recent Advances in the Synthesis of Bowl-Shaped Aromatic Compounds. *Synlett* **2013**, *24*, 1316–1321.
12. Muzammil, E. M.; Halilovic, D.; Stuparu, M. C. Synthesis of Corannulene-Based Nanographenes. *Commun. Chem.* **2019**, *2*, 58.
13. Pun, S. H.; Miao, Q. Toward Negatively Curved Carbons. *Acc. Chem. Res.* **2018**, *51*, 1630–1642.
14. Márquez, I. R.; Castro-Fernandez, S.; Millán, A.; Campaña, A. G. Synthesis of Distorted Nanographenes Containing Seven- and Eight-Membered Carbocycles. *Chem. Commun.* **2018**, *54*, 6705–6718.
15. Ball, M.; Zhong, Y.; Wu, Y.; Schenck, C.; Ng, F.; Steigerwald, M.; Xiao, S.; Nuckolls, C. Contorted Polycyclic Aromatics. *Acc. Chem. Res.* **2015**, *48*, 267–276.
16. Shen, Y.; Chen, C. Helicenes: Synthesis and Applications. *Chem. Rev.* **2012**, *112*, 1463–1535.
17. Li, C.; Yang, Y.; Miao, Q. Recent Progress in Chemistry of Multiple Helicenes, *Chem. Asian J.* **2018**, *13*, 884–894.
18. Tsurosaki, A.; Kamikawa, K. Multiple Helicenes Featuring Synthetic Approaches and Molecular Structures. *Chem. Lett.* **2021**, *50*, 1913–1932.
19. Cheung, K.-Y.; Segawa, Y.; Itami, K. Synthetic Strategies of Carbon Nanobelts and Related Belt-Shaped Polycyclic Aromatic Hydrocarbons. *Chem. Eur. J.* **2020**, *26*, 14791–14801.
20. Simpson, C. D.; Brand, J. D.; Berresheim, A. J.; Przybilla, L.; Räder, H. J.; Müllen, K. Synthesis of a Giant 222 Carbon Graphite Sheet. *Chem. Eur. J.* **2002**, *8*, 1424–1429.
21. Simpson, C. D.; Mattersteig, G.; Martin, K.; Gherghel, G. L.; Bauer, R. E.; Räder, H. J.; Müllen, K. Nanosized Molecular Propellers by Cyclodehydrogenation of Polyphenylene Dendrimers. *J. Am. Chem. Soc.* **2004**, *126*, 3139–3147.
22. Ernst, K.-H. Molecular Chirality at Surfaces. *Phys. Status Solidi B* **2012**, *249*, 2057–2088.
23. Ernst, K.-H.; Baumann, S.; Lutz, C. P.; Seibel, J.; Zoppi, L.; Heinrich, A. J. Pasteur's Experiment Performed at the Nanoscale: Manual Separation of Chiral Molecules, One by One. *Nano Lett.* **2015**, *15*, 5388–5392.
24. Gross, L.; Mohn, F.; Moll, N.; Liljeroth, P.; Meyer, G. The Chemical Structure of a Molecule Resolved by Atomic Force Microscopy. *Science* **2009**, *325*, 1110–1114.
25. Gross, L.; Schuler, B.; Pavliček, N.; Fatayer, S.; Majzik, Z.; Moll, N.; Peña, D.; Meyer, G. Atomic Force Microscopy for Molecular Structure Elucidation. *Angew. Chem. Int. Ed.* **2018**, *57*, 3888–3908.
26. Zhong, Q.; Li, X.; Zhang, H.; Chi, L. Noncontact Atomic Force Microscopy: Bond Imaging and Beyond. *Surf. Sci. Rep.* **2020**, *75*, 100509.

DOI: 10.31635/ccschem.023.202303065
Citation: *CCS Chem.* **2023**, 5, 2888–2896
Link to VoR: https://doi.org/10.31635/ccschem.023.202303065

27. Gross, L.; Mohn, F.; Moll, N.; Schuler, B.; Ado, A. C.; Guitián, E.; Peña, D.; Gourdon, A.; Meyer, G. Bond-Order Discrimination by Atomic Force Microscopy. *Science* **2012**, *337*, 1326–1329.
28. Ebeling, D.; Šekutor, M.; Stiefermann, M.; Tschakert, J.; Dahl, J. E. P.; Carlson, R. M. K.; Schirmeisen, A.; Schreiner, P. R. Assigning the Absolute Configuration of Single Aliphatic Molecules by Visual Inspection. *Nat. Commun.* **2018**, *9*, 2420.
29. Ebeling, D.; Šekutor, M.; Stiefermann, M.; Tschakert, J.; Dahl, J. E. P.; Carlson, R. M. K.; Schirmeisen, A.; Schreiner, P. R. Assigning the Absolute Configuration of Single Aliphatic Molecules by Visual Inspection. London Dispersion Directs On-Surface Self-Assembly of [121]Tetramantane Molecules. *ACS Nano* **2017**, *11*, 9459–9466.
30. Albrecht, F.; Pavliček, N.; Herranz-Lancho, C.; Ruben, M.; Repp, J. Characterization of a Surface Reaction by Means of Atomic Force Microscopy. *J. Am. Chem. Soc.* **2015**, *137*, 7424–7428.
31. Schuler, B.; Liu, W.; Tkatchenko, A.; Moll, N.; Meyer, G.; Mistry, A.; Fox, D.; Gross, L. Adsorption Geometry Determination of Single Molecules by Atomic Force Microscopy. *Phys. Rev. Lett.* **2013**, *111*, 106103.
32. Martin-Jimenez, D.; Ahles, S.; Mollenhauer, D.; Wegner, H. A.; Schirmeisen, A.; Ebeling, D. Bond-Level Imaging of the 3D Conformation of Adsorbed Organic Molecules Using Atomic Force Microscopy with Simultaneous Tunneling Feedback. *Phys. Rev. Lett.* **2019**, *122*, 196101.
33. Pozo, I.; Majzik, Z.; Pavliček, N.; Melle-Franco, M.; Guitián, E.; Peña, D.; Gross, L.; Pérez, D. Revisiting Kekulene: Synthesis and Single-Molecule Imaging. *J. Am. Chem. Soc.* **2019**, *141*, 15488–15493.
34. Rickhaus, M.; Mayor, M.; Juríček, M. Chirality in Curved Polyaromatic Systems. *Chem. Soc. Rev.* **2017**, *46*, 1643–1660.
35. de Oteyza, D. G.; García-Lekue, A.; Vilas-Varela, M.; Merino-Díez, N.; Carbonell-Sanromà, E.; Corso, M.; Vasseur, G.; Rogero, C.; Guitián, E.; Pascual, J. I.; Ortega, J. E.; Wakayama, Y.; Peña, D. Substrate-Independent Growth of Atomically Precise Chiral Graphene Nanoribbons. *ACS Nano* **2016**, *10*, 9000–9008.
36. Urgel, J. I.; Giovannantonio, M. D.; Segawa, Y.; Ruffieux, P.; Scott, L. T.; Pignedoli, C. A.; Itami, K.; Fasel, R. Negatively Curved Warped Nanographene Self-Assembled on Metal Surface. *J. Am. Chem. Soc.* **2019**, *141*, 13158–13164.
37. Xiao, W.; Ernst, K.-H.; Palotas, K.; Zhang, Y.; Bruyer, E.; Peng, L.; Greber, T.; Hofer, W. A.; Scott, L. T.; Fasel, R. Microscopic Origin of Chiral Shape Induction in Achiral Crystals. *Nat. Chem.* **2016**, *8*, 326–330.
38. Maïrena, A.; Mendelita, J. I.; Setsovych, O.; Trefort, A.; Stará, I. G.; Stary, I.; Jelínek, P.; Ernst, K.-H. Heterochiral Recognition Among Functionalized Heptahelicenes on Noble Metal Surfaces. *Chem. Commun.* **2019**, *55*, 10595–10598.
39. Wang, Y.; Allemann, O.; Balaban, T. S.; Vanthuyne, N.; Liden, A.; Baldridge, K. K.; Siegel, J. S. Chiral Atropisomeric Indenocorannulene Bowls: Critique of the Cahn–Ingold–Prelog Conception of Molecular Chirality. *Angew. Chem Int. Ed.* **2018**, *57*, 6470.
40. Topolinski, B.; Schmidt, B. M.; Kathan, M.; Troyanov, S. I.; Lentz, D. Corannulenylferrocenes: Towards a 1D, Non-Covalent Metal–Organic Nanowire. *Chem. Commun.* **2012**, *48*, 6298–6300.
41. Yanney, M.; Fronczek, F. R.; Henry, W. P.; Beard, D. J.; Sygula, A. Cyclotrimerization of Corannulyne: Steric Hindrance Tunes the Inversion Barriers of Corannulene Bowl. *Eur. J. Org. Chem.* **2011**, *2011*, 6636–6639.
42. Fujikawa, T.; Preda, D. V.; Segawa, Y.; Itami, K.; Scott, L. T. Corannulene–Helicene Hybrids: Chiral π-Systems Comprising Both Bowl and Helical Motifs. *Org. Lett.* **2016**, *18*, 3992.
43. Kato, K.; Segawa, Y.; Itami, K. Symmetric Multiple Carbohelicenes. *Synlett* **2019**, *30*, 370–377.
44. Kawai, S.; Nishiuchi, T.; Kodama, T.; Spijker, P.; Pawlak, R.; Meier, T.; Tracey, J.; Kubo, T.; Meyer, E.; Foster, A. S. Direct Quantitative Measurement of the C═O···H–C Bond by Atomic Force Microscopy. *Sci. Adv.* **2017**, *3*, e1603258.
45. Shu, C.-H.; Liu, M.-X.; Zha, Z.-Q.; Pan, J.-L.; Zhang, S.-Z.; Xie, Y.-L.; Chen, J.-L.; Yuan, D.-W.; Qiu, X.-H.; Liu, P.-N. On-Surface Synthesis of Poly(p-phenylene ethynylene) Molecular Wires via in Situ Formation of Carbon-Carbon Triple Bond. *Nat Commun.* **2018**, *9*, 2322.
46. Ebeling, D.; Zhong, Q.; Schlöder, T.; Tschakert, J.; Henkel, P.; Ahles, S.; Chi, L.; Mollenhauer, D.; Wegner, H. A.; Schirmeisen, A. Adsorption Structure of Mono- and Diradicals on a Cu(111) Surface: Chemoselective Dehalogenation of 4-Bromo-3″-iodo-p-terphenyl. *ACS Nano* **2019**, *13*, 324–336.
47. Parschau, M.; Fasel, R.; Ernst, K.-H.; Gröning, O.; Brandenberger, L.; Schillinger, R.; Greber, T.; Seitsonen, A. P.; Wu, Y.-T.; Siegel, J. S. Buckybowls on Metal Surfaces: Symmetry Mismatch and Enantiomorphism of Corannulene on Cu(110). *Angew. Chem. Int. Ed.* **2007**, *46*, 8258–8261.
48. Hamada, I. van der Waals Density Functional Made Accurate. *Phys. Rev. B* **2014**, *89*, 121103.
49. Hapala, P.; Kichin, G.; Wagner, C.; Tautz, F. S.; Temirov, R.; Jelínek, P. Mechanism of High-Resolution STM/AFM Imaging with Functionalized Tips. *Phys. Rev. B* **2014**, *90*, 085421.
50. Szumna, A. Inherently Chiral Concave Molecules—From Synthesis to Applications. *Chem. Soc. Rev.* **2010**, *39*, 4274–4285.
51. Bertucci, C.; Tedesco, D. Advantages of Electronic Circular Dichroism Detection for the Stereochemical Analysis and Characterization of Drugs and Natural Products by Liquid Chromatography. *J. Chromatograp. A* **2012**, *1269*, 69–81.
52. Szwed, K.; Górecki, M.; Frelek, J.; Asztemborska, M. Enantioselective Extraction System Containing Binary Chiral Selectors and Chromatographic Enantioseparation Method for Determination of the Absolute Configuration of Enantiomers of Cyclopentolate. *Chromatographia* **2013**, *76*, 1603–1611.
53. Górecki, M.; Roszkowski, P.; Błachut, D.; Maurin, J. K.; Budzianowski, A.; Frelek, J.; Czarnocki, Z. Atropoisomerism in Mono- and Diaryl-Substituted 4-Amino-2,6-lutidines. *Eur. J. Org. Chem.* **2016**, *2016*, 2966–2971.

DOI: 10.31635/ccschem.023.202303065
Citation: *CCS Chem.* **2023**, 5, 2888–2896
Link to VoR: https://doi.org/10.31635/ccschem.023.202303065